PASJ: Publ. Astron. Soc. Japan **60**, 23–35, 2008 February 25

Mapping Observations of 6.7 GHz Methanol Masers with the Japanese VLBI Network

Koichiro SUGIYAMA,[1] Kenta FUJISAWA,[2] Akihiro DOI,[2,3] Mareki HONMA,[4,5] Hideyuki KOBAYASHI,[4,6] Takeshi BUSHIMATA,[4,7] Nanako MOCHIZUKI,[3] and Yasuhiro MURATA[3,8]

[1]*Graduate school of Science and Engineering, Yamaguchi University, 1677-1 Yoshida, Yamaguchi, Yamaguchi 753-8512*
[2]*Department of Physics, Faculty of Science, Yamaguchi University, 1677-1 Yoshida, Yamaguchi, Yamaguchi 753-8512*
[3]*The Institute of Space and Astronautical Science, Japan Aerospace Exploration Agency, 3-1-1 Yoshinodai, Sagamihara, Kanagawa 229-8510*
[4]*VERA Project, National Astronomical Observatory of Japan, 2-21-1 Osawa, Mitaka, Tokyo 181-8588*
[5]*Department of Astronomical Science, Graduate University for Advanced Studies, 2-21-1 Osawa, Mitaka, Tokyo 181-8588*
[6]*Mizusawa VERA Observatory, National Astronomical Observatory of Japan, 2-12 Hoshigaoka, Mizusawa, Oshu, Iwate 023-0861*
[7]*Space VLBI Project, National Astronomical Observatory of Japan, 2-21-1 Osawa, Mitaka, Tokyo 181-8588*
[8]*Department of Space and Astronautical Science, The Graduate University for Advanced Studies, 3-1-1 Yoshinodai, Sagamihara, Kanagawa 229-8510*
j011vc@yamaguchi-u.ac.jp

(Received 2007 May 16; accepted 2007 September 10)

Abstract

We have observed 13 methanol maser sources associated with massive star-forming regions: W 3(OH), Mon R2, S 255, W 33A, IRAS 18151−1208, G 24.78+0.08, G 29.95−0.02, IRAS 18556+0136, W 48, OH 43.8−0.1, ON 1, Cep A, and NGC 7538 at 6.7 GHz using the Japanese VLBI Network (JVN). Twelve of the thirteen sources were detected at our longest baseline of $\sim 50\,\mathrm{M}\lambda$, and their images are presented. Seven of them are the first VLBI images at 6.7 GHz. The high detection rate and the small fringe spacing of ~ 4 mas suggest that most of the methanol maser sources have compact structures. Given this compactness as well as the known properties of long life and small internal motion, the methanol maser line is suitable for astrometry with VLBI.

Key words: masers: methanol — techniques: interferometric — very-long-baseline interferometry (VLBI)

1. Introduction

Class II methanol masers are well-known as tracers of early stages of high-mass star formation (Walsh et al. 1998; Minier et al. 2001; Ellingsen 2006). Classes I and II are defined on the basis of associated sources (Batrla et al. 1987; Menten 1991a); different pumping mechanisms are proposed for them (Cragg et al. 1992; Sobolev et al. 1997). The class II maser is represented by 6.7 and 12.2 GHz lines (Batrla et al. 1987; Menten 1991b). The spot size of class II masers is several AU (Menten et al. 1992; Moscadelli et al. 1999), while the class I maser is resolved with the very long baseline interferometric (VLBI) technique (Lonsdale et al. 1998).

VLBI observations for astrometry with hydroxyl, water, and methanol masers have been made using a phase referencing technique. The accuracy of measuring with hydroxyl masers is ~ 1 mas (Vlemmings et al. 2003), while that which achieved with water masers is up to a few tens of μas (Hachisuka et al. 2006). Xu et al. (2006) have also achieved a positional accuracy of $\sim 10\,\mu$as with a methanol maser at 12.2 GHz. This has been the only one astrometric observation with methanol masers. Internal proper motions are often measured typically at a few mas per year for water masers at 22 GHz (e.g., Genzel et al. 1981a, b); this motion sometimes prevents us from making a distinction of the annual parallax and the internal proper motion. The internal proper motion for class II methanol masers is small, and has been measured only for W 3(OH) at 12.2 GHz (Moscadelli et al. 2002). The lifetime of 22 GHz water masers is sometimes too short for measuring the annual parallax. For example, several spots disappear after a month's interval in Cepheus A and IRAS 21391+5802 (Patel et al. 2000; Torrelles et al. 2001a, b). A monitoring of the variability of the 6.7 GHz methanol line for 4 yr showed that each spectral feature survives regardless of some variabilities (Goedhart et al. 2004); namely, the lifetime of this maser is usually long enough for measuring the annual parallax. There are 519 sites of 6.7 GHz methanol masers in a list compiled by Pestalozzi, Minier, and Booth (2005). Recently, 48 new sources have been detected using the 305 m Arecibo radio telescope (Pandian et al. 2007). For the above reasons, i.e., compactness, small internal proper motion, long life, and a large number of known sources, class II methanol masers may also be a useful probe for astrometry.

The VLBI Exploration of Radio Astrometry (VERA: Kobayashi et al. 2003) is a dedicated VLBI network, which mainly observes Galactic water masers for measuring their distances and motions. Methanol masers at 6.7 GHz as well as water masers would also contribute to revealing the Galactic structure. The spot size of a methanol maser should be small enough for high-precision astrometry. Studies of the spot

Table 1. Sample of 6.7 GHz methanol masers.

Source	Coordinates (J2000.0)		Ref.	S_p	d	VLBI obs.
	RA (h m s)	Dec (° ′ ″)		(Jy)	(kpc)	
W 3(OH)	02 27 03.820	61 52 25.40	10	3294	1.95	1
Mon R2	06 07 47.867	−06 22 56.89	4	104	0.83	6, 7
S 255	06 12 54.024	17 59 23.01	6	79	2.5	6, 7
W 33A	18 14 39.52	−17 51 59.7	13	297	4.0	...
IRAS 18151−1208	18 17 58.07	−12 07 27.2	13	119	3.0	8
G 24.78+0.08	18 36 12.57	−07 12 11.4	*	84	7.7	...
G 29.95−0.02	18 46 03.741	−02 39 21.43	6	182	9.0	...
IRAS 18556+0136	18 58 13.1	01 40 35	12	191	2.0	...
W 48	19 01 45.5	01 13 28	3	733	3.4	6
OH 43.8−0.1	19 11 53.987	09 35 50.308	2	51	2.8	...
ON 1	20 10 09.1	31 31 34	12	107	1.8	...
Cep A	22 56 17.903	62 01 49.65	13	371	0.73	...
NGC 7538	23 13 45.364	61 28 10.55	6	256	2.8	5, 6, 7, 9, 11

Column 1: Source name; Columns 2–3: Coordinates in J2000.0; Column 4: Reference of coordinates; Column 5: Peak flux densities from the single-dish observation by Yamaguchi 32 m telescope; Column 6: Source distance; Column 7: Published VLBI observations at 6.7 GHz.

References — (1) Menten et al. (1992); (2) Kurtz, Churchwell, and Wood (1994); (3) Caswell et al. (1995a); (4) Walsh et al. (1998); (5) Minier, Booth, and Conway (1998); (6) Minier, Booth, and Conway (2000); (7) Minier, Conway, and Booth (2001); (8) Voronkov et al. (2002); (9) Pestalozzi et al. (2004); (10) Etoka, Cohen, and Gray (2005); (11) Pestalozzi et al. (2006); (12) Joint IRAS Science W.G. 1988; (13) Fringe rate mapping in our observations (accuracy of position is 100–300 mas).

* The coordinates of this source are not used for this data reduction. These coordinates are obtained from the observations made in the following year. They are coincident with the coordinates in the catalog listed by Pestalozzi, Minier, and Booth (2005).

size, however, have been made for only a few cases so far. The number of sources imaged with a baseline of $\geq$50 Mλ at 6.7 GHz was only four (Menten et al. 1992; Bartkiewicz et al. 2005; Pestalozzi et al. 2006; Goddi et al. 2007). Minier, Booth, and Conway (2002) discussed the size and structure of an individual masing region in detail based on their 6.7 and 12.2 GHz observations. They showed that the majority of the masing regions consist of a compact maser core surrounded by extended emission (halo), and derived a core size of 2 to 20 AU.

We have started investigations of methanol masers using the Japanese VLBI Network (JVN) for astrometry. This is a newly established network with 50–2560 km baselines across the Japanese islands (Doi et al. 2006a), and consists of ten antennas, including four radio telescopes of VERA. We installed 6.7 GHz receivers on three telescopes of the JVN and made a snap-shot imaging survey toward thirteen sources associated with massive star-forming regions. The aims of these observations are to investigate the detectability of 6.7 GHz masers with our longest baseline of $\sim$50 Mλ, corresponding to a fringe spacing of $\sim$4 mas, and to verify the imaging capability of this network.

In this paper, we describe the details of this observations and data reduction in section 2. In section 3 we present images of the detected sources, and report on the results of each individual source. Finally, we discuss the properties of this maser for astrometry in section 4, based on the results of this observation.

2. Observations and Data Reduction

2.1. VLBI Observation

The $5_1 \rightarrow 6_0 A^+$ methanol transition at 6668.518 MHz was observed on 2005 September 26 from 5:00 to 21:00 UT using three telescopes (Yamaguchi 32 m, and VERA-Mizusawa 20 m, VERA-Ishigaki 20 m) of the JVN. The maximum fringe spacing was 9.1 mas (Yamaguchi–Mizusawa, 22 Mλ) and the minimum was 4.1 mas (Mizusawa–Ishigaki, 50 Mλ). Right-circular polarization was received at Yamaguchi with the system noise temperature of 220 K, while linear polarization was received at the Mizusawa and Ishigaki stations with the system noise temperature of 120 K. The data were recorded on magnetic tapes using the VSOP-terminal system at a data rate of 128 Mbps with 2-bit quantization and 2 channels, and correlated at the Mitaka FX correlator (Shibata et al. 1998). From the recorded 32 MHz bandwidth, 8 MHz (6664 MHz to 6672 MHz) was divided into 1024 channels and used for data analysis, yielding a velocity resolution of 0.35 km s^{-1}.

Bright sources with widespread-velocity range were selected as targets of this observation. The following thirteen sources were observed: W 3(OH), Mon R2, S 255, W 33A, IRAS 18151−1208, G 24.78+0.08, G 29.95−0.02, IRAS 18556+0136, W 48, OH 43.8−0.1, ON 1, Cep A, and NGC 7538. The details of each source are given in table 1. Scans of 15 min duration were made 2–4 times on each source at different hour angles in order to improve the uv-coverages. The number of scans for each source is given in table 2. Strong continuum sources (NRAO 530, 3C 454.3, and 3C 84) were

Table 2. Observational results.

Source	$N_{\rm scan}$	$\theta_{\rm maj}\times\theta_{\rm min}$ (mas × mas)	PA (°)	σ (Jy beam^{-1})	$v_{\rm ref}$ (km s^{-1})	$S^{\rm p}_{\rm VLBI}/S^{\rm p}$ (%)	$S_{\rm VLBI}/S$ (%)
W 3(OH)	3	5.5×2.3	131	0.24	−45.46	31	45
Mon R2	2	19.3×2.1	140	0.30	10.64	24	33
S 255	2	19.4×2.1	144	...	...	...	...
W 33A	3	12.6×2.5	138	0.37	39.69	45	51
IRAS 18151−1208	3	10.9×2.5	138	0.63	27.83	84	208
G 24.78+0.08	3	9.5×2.4	135	0.28	113.43	33	27
G 29.95−0.02	2	19.5×2.2	139	0.46	96.10	86	78
IRAS 18556+0136	3	9.4×2.5	135	0.32	28.57	37	36
W 48	3	12.2×3.0	99	0.67	42.45	68	91
OH 43.8−0.1	2	16.2×2.2	139	0.36	39.48	18	30
ON 1	4	4.3×2.5	112	0.23	−0.07	4	27
Cep A	4	4.1×2.6	87	0.62	−2.56	86	65
NGC 7538	4	3.9×2.5	95	0.20	−56.10	69	30

Column 1: source name; Column 2: number of scans; Column 3: FWHMs of major and minor axes of synthesized beam; Column 4: position angle of major axis of beam; Column 5: rms of image noise in a line-free channel; Column 6: reference velocity channel; Column 7: flux ratio of the correlated to the total-power spectra at the peak channel of total spectra; Column 8: flux ratio of the correlated to the total-power spectra of the integrated spectra.

observed every 2 hr for bandpass and delay calibration.

The data were reduced using the Astronomical Image Processing System (AIPS: Greisen 2003). Correlator digitization errors were corrected using the task ACCOR. Clock offsets and clock-rate offsets were corrected using strong continuum calibrators in the task FRING. Bandpass calibration was performed using strong continuum calibrators in the task BPASS. Doppler corrections were made by running the tasks SETJY and CVEL. Amplitude calibration parameters were derived from the total-power spectra of maser lines using the template method in the task ACFIT. Fringe-fitting was conducted using one spectral channel including a strong maser feature in the task FRING. The solutions were applied to all of the other channels.

We searched maser spots over an area of $4\farcs0\times4\farcs0$ with the Difmap software (Shepherd 1997). Structure models were made by model fitting with point sources and self-calibration algorithms iteratively. The phase solutions of self-calibration were applied to all of the other channels.

In addition to the above-mentioned analysis, special amplitude calibrations were necessary for the reduction because different polarizations (circular/linear) were correlated. Since a visibility amplitude is reduced by $1/\sqrt{2}$ in correlation between linear and single circular polarizations, the factor was corrected. In the case of linear and linear polarizations, the amplitude varies with time, depending on the position angle between the antennas. Amplitude-correction factors were calculated for each observational scan and applied to the visibilities. We made a baseline-based correction on each observational scan. The correction procedure was confirmed in some observations on different days by applying the task BLCAL for bright continuum sources. This process indicated that the accuracy of this calibration was $\sim10\%$.

2.2. *Spectroscopic Single-Dish Observation*

We have also made a series of single-dish observations of a 6.7 GHz methanol maser with Yamaguchi 32 m telescope. The single-dish observations were made about one month before the VLBI observation (2005 August). In this paper, we use the spectra as the total-power (not cross-correlated) spectra in comparison with the cross-correlated spectra. The accuracy of the correlated flux density depends on the accuracy of the single-dish observation.

The received signal at dual circular polarizations with a bandwidth of 4 MHz each was divided into 4096 channels, yielding a velocity resolution of 0.044 km s^{-1}. The flux density calibration was made using an aperture efficiency of 70% and a system noise temperature (220 K) measured on the first day of the single-dish observation. The accuracy of the calibration was 10%. The rms of the noise was typically 1.0 Jy, for data combined from dual polarizations with a 14 min integration. We used source positions listed in the IRAS Point Source Catalog (PSC: Joint IRAS Science W.G. 1988). The error in the LSR velocity was potentially ±0.3 km s^{-1}.

3. Results

All of the targets, except for S 255, were detected. The VLBI maps of the detected sources are presented in figures 1–13. Only the total-power spectrum is shown in figure 3 for S 255. The maps indicate positions of the maser spots relative to that of the reference spot; the size and color of a spot represent its flux density in logarithmic scale and its radial velocity, respectively. Correlated spectra (total CLEANed components) are shown in addition to the total-power spectra for each source. The rms of the image noise in a line-free channel ranges from 200 to 670 mJy beam^{-1}. The minimum detectable sensitivities of 7σ were in the range of 1.4 to 4.7 Jy beam^{-1}. The maximum dynamic range was 196 for W 3(OH). The projected baseline

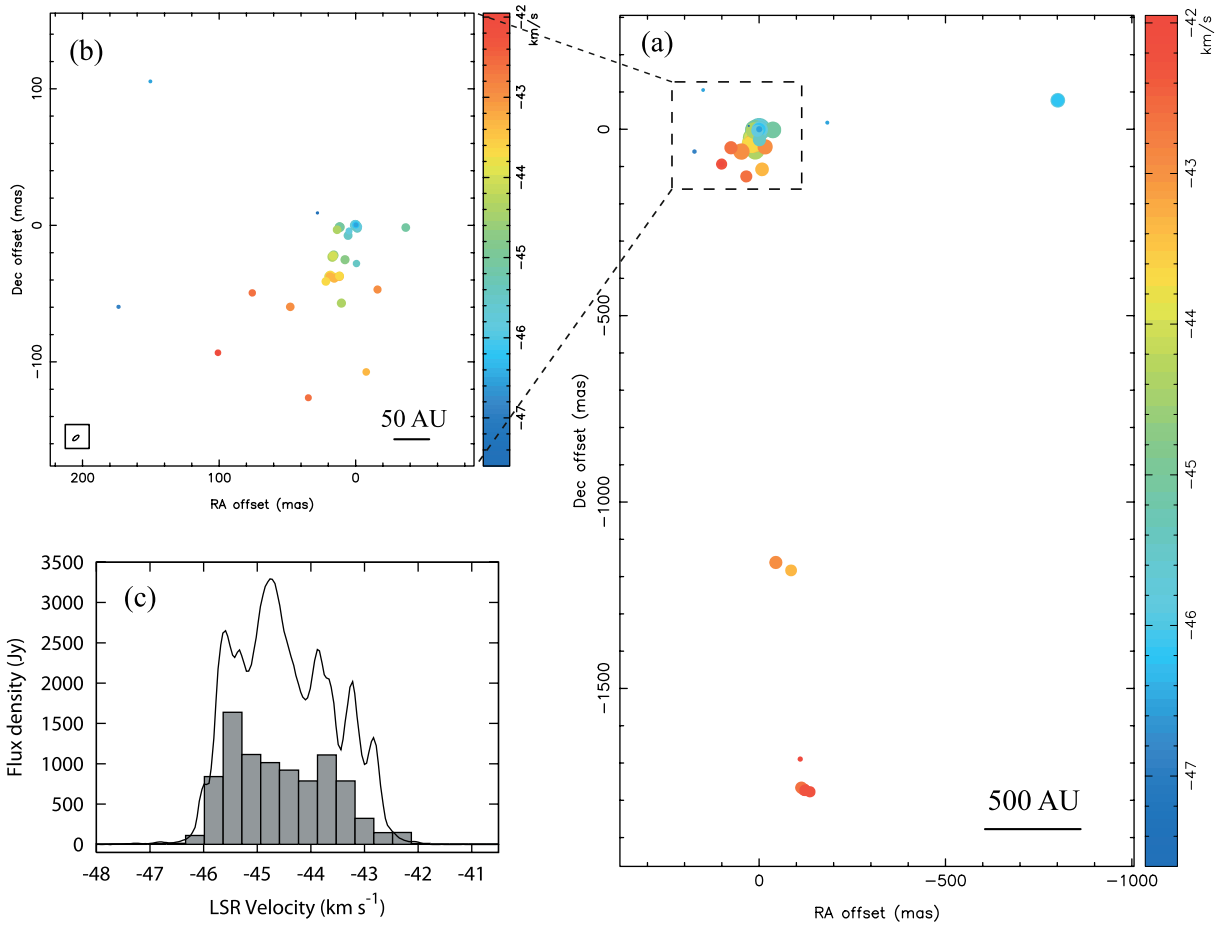

Fig. 1. W 3(OH): (a) Wide field view of a $0\farcs9 \times 1\farcs8$ map. (b) Close-up of the main cluster. (c) CLEANed component spectrum (filled block) and total spectrum (solid curve).

ranged from 11 to 50 Mλ for all sources, except for W 33A, IRAS 18151−1208, and G 24.78+0.08 (7 to 50 Mλ). The flux ratio between the correlated and the total-power spectra at the peak channel of the total spectra and that of the integrated spectra are shown in columns 7 and 8 in table 2, respectively. The ratio of the correlated flux densities at the longest baseline of 50 Mλ to that at zero-baseline (total-power) was 20% on average. We describe the results concerning each individual source below in order of right ascension.

3.1. *W 3(OH)*

W 3(OH) (figure 1) is a well-studied star-forming region at a distance of 1.95 ± 0.04 kpc (Xu et al. 2006) containing a hot molecular core (HMC) and an ultra compact (UC) H II region (Turner & Welch 1984). The central object is thought to be an O9−O7 young star with an estimated mass of $\simeq$ 30 $M_\odot$ (Dreher & Welch 1981). W 3(OH) has been imaged with the Multi-Element Radio-Linked Interferometer Network (MERLIN: Etoka et al. 2005; Vlemmings et al. 2006; Harvey-Smith & Cohen 2006) and VLBI array at 6.7 GHz (Menten et al. 1992), and with the VLBA at 12.2 GHz (Menten et al. 1988; Moscadelli et al. 1999, 2002, 2003; Xu et al. 2006).

In our observation, 48 maser spots were detected. The velocity of the reference feature is −45.46 km s^{-1} (−45.37 km s^{-1} appeared in Etoka et al. 2005). We detected maser clusters 1, 5, 6, and 7 defined by Menten et al. (1992), and found a new spot of −46.51 km s^{-1}, 180 mas west from the reference feature. There are 38 spots within a 200 mas area of cluster 6. The other three clusters are located $0\farcs8$ west, $1\farcs2$ south, and $1\farcs7$ south of the main cluster.

3.2. *Mon R2*

The Monoceros R2 (Mon R2, figure 2) molecular cloud has a cluster of seven bright infrared sources (Beckwith et al. 1976). The cluster is one of the closest massive star-forming regions to the solar system at a distance of 830 pc (Racine 1968; Herbst & Racine 1976). The 6.7 GHz methanol maser of Mon R2 has been observed with the Australia Telescope Compact Array (ATCA: Walsh et al. 1998) and with the European VLBI Network (EVN: Minier et al. 2000, 2001). Although there are several peaks in the total-power spectrum, our VLBI observation detected only one spectral feature around 10.64 km s^{-1} as eight maser spots. These eight spots ($V_{\rm lsr}$ = 10.29 to 11.34 km s^{-1}) correspond to C (identifying letter) defined by Walsh et al. (1998), and are also identified with five of the fourteen spots detected by Minier, Booth, and

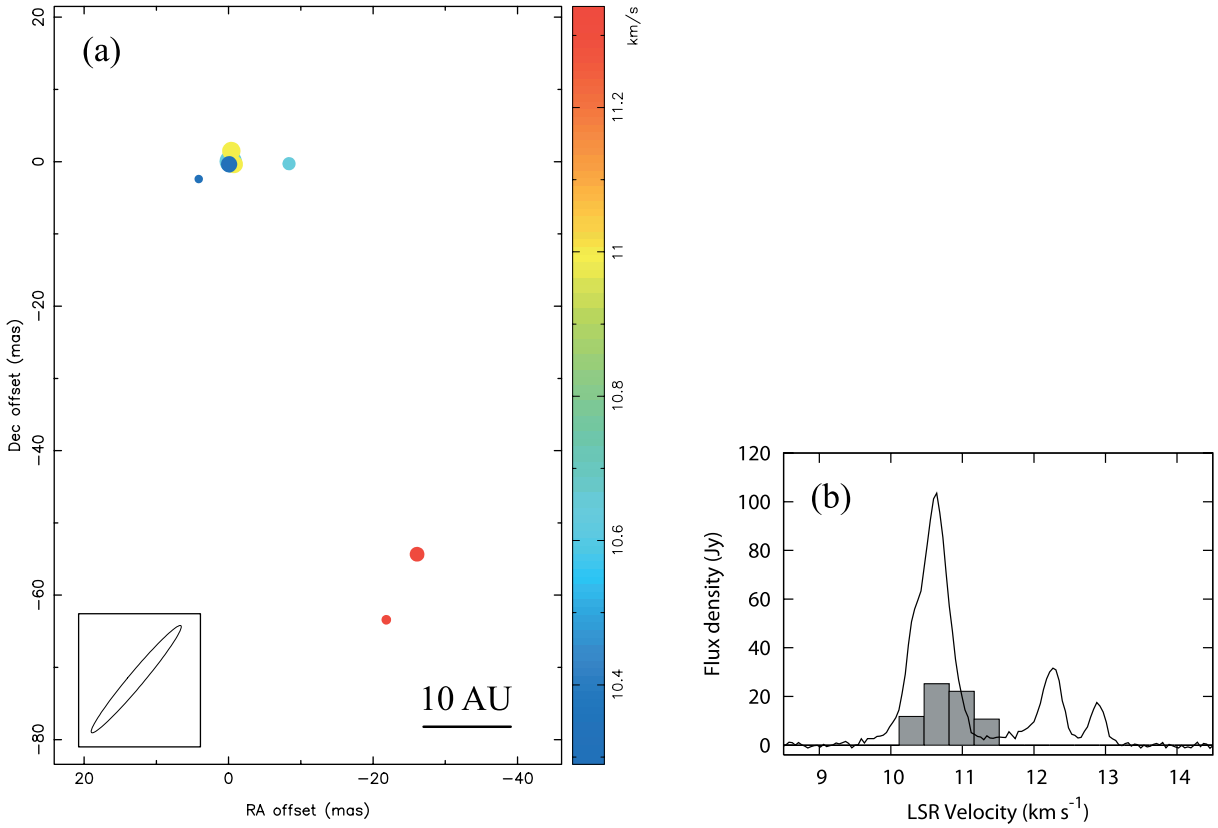

Fig. 2. Mon R2: (a) Map. (b) CLEANed component spectrum (filled block) and total spectrum (solid curve).

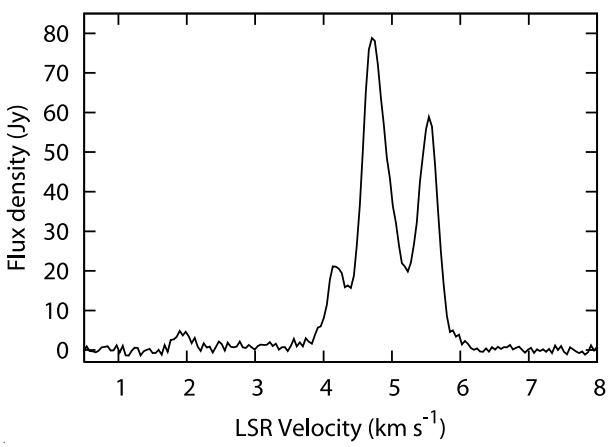

Fig. 3. Total spectrum of S 255 observed by Yamaguchi 32 m telescope. This source was not detected by our VLBI observation.

Conway (2000).

Since this source shows an ongoing flux variation, the single-dish spectrum was largely different from that of previous observations. It seems that some spectral features disappeared and some others appeared during the period from 1992 to 2005 (Caswell et al. 1995a; Szymczak et al. 2000).

3.3. S 255

S 255, located at a distance of 2.5 kpc (Mezger et al. 1988), includes one UC H II region, G 192.58–0.04 (Kurtz et al. 1994). S 255 was observed with the EVN at 6.7 GHz (Minier et al. 2000, 2001), and seven spots were detected with the longest projected baseline of $\sim 30\,\mathrm{M}\lambda$. We observed this source, and correlated it with the coordinates used by Minier, Booth, and Conway (2000) and Minier, Conway, and Booth (2001), but no spot was detected. This source might be resolved with our baselines. The single-dish spectrum observed by Yamaguchi 32 m telescope is shown in figure 3.

3.4. W 33A

W 33A (figure 4) is a highly luminous object ($L = 1{\times}10^5\ L_\odot$: Stier et al. 1984) and coincides with deeply embedded massive young stars (van der Tak et al. 2000). The kinematic distance based on CS and $C^{34}S$ observations is 4 kpc (van der Tak et al. 2000). A map consisting of eleven maser spots was obtained with the ATCA (Walsh et al. 1998).

Our observation, the first VLBI for this source, detected 19 maser spots that correspond to F, G, and K, defined by the ATCA observation. The total-power spectrum has several peaks, but weak spectral peaks were not detected in the VLBI map. This source consists of two clusters, and all of the clusters are separated by more than 1000 AU.

3.5. IRAS 18151−1208

IRAS 18151−1208 (figure 5) is embedded in a high-density cloud (Bronfman et al. 1996), and is thought to be in a pre-UC H II phase (Davis et al. 2004). The kinematic distance, based on a CS line observation, is 3.0 kpc (Brand & Blitz 1993). Thirteen maser spots were detected by our observation. This

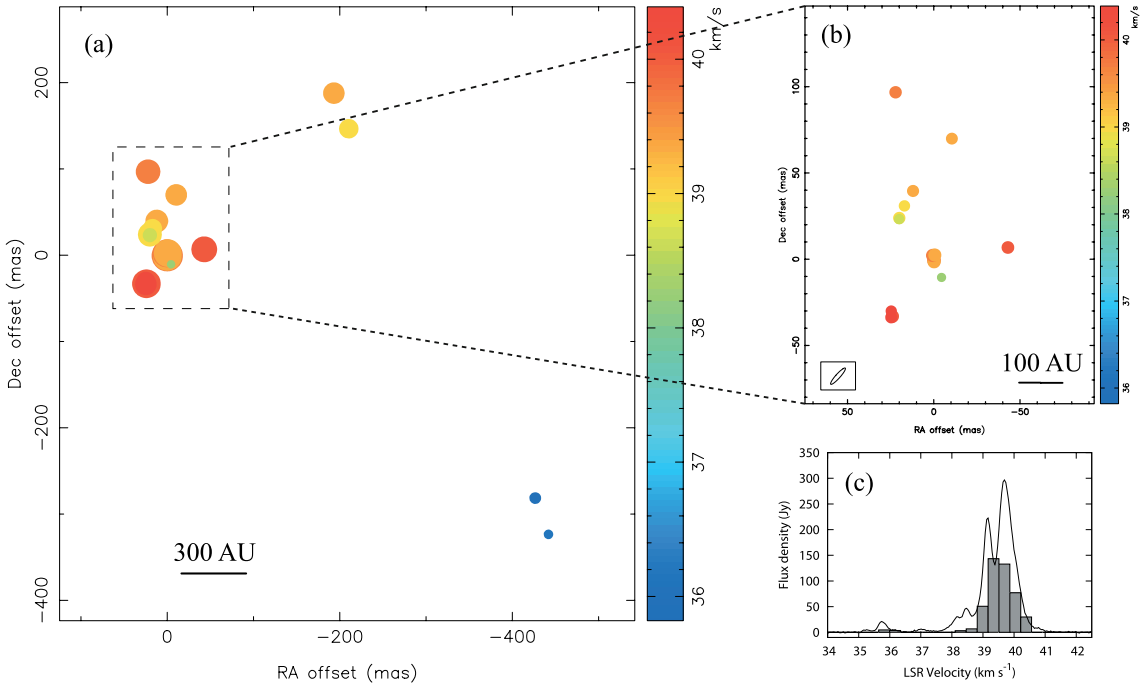

Fig. 4. W 33A: (a) Wide field view of a $0.''5 \times 0.''5$ map. (b) Close-up of the main cluster. (c) CLEANed component spectrum (filled block) and total spectrum (solid curve).

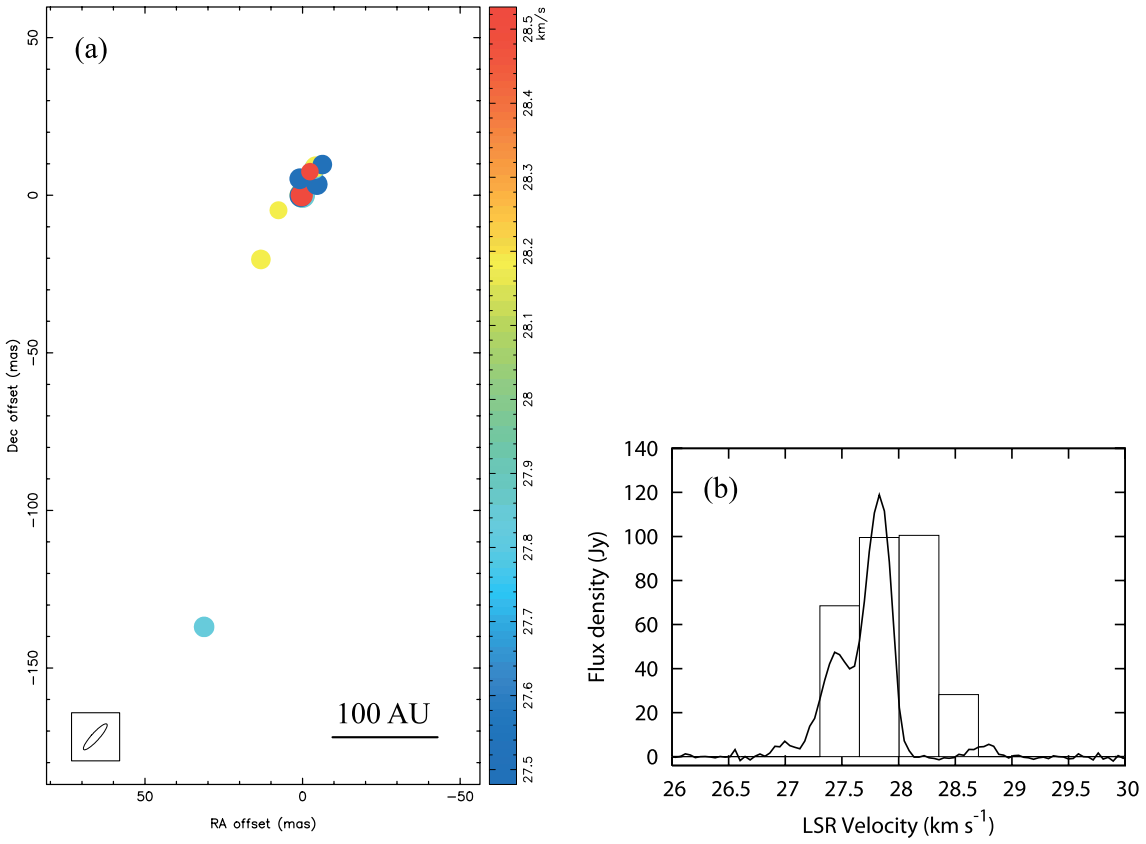

Fig. 5. IRAS 18151−1208: (a) Map. (b) CLEANed component spectrum (blank block) and total spectrum (solid curve).

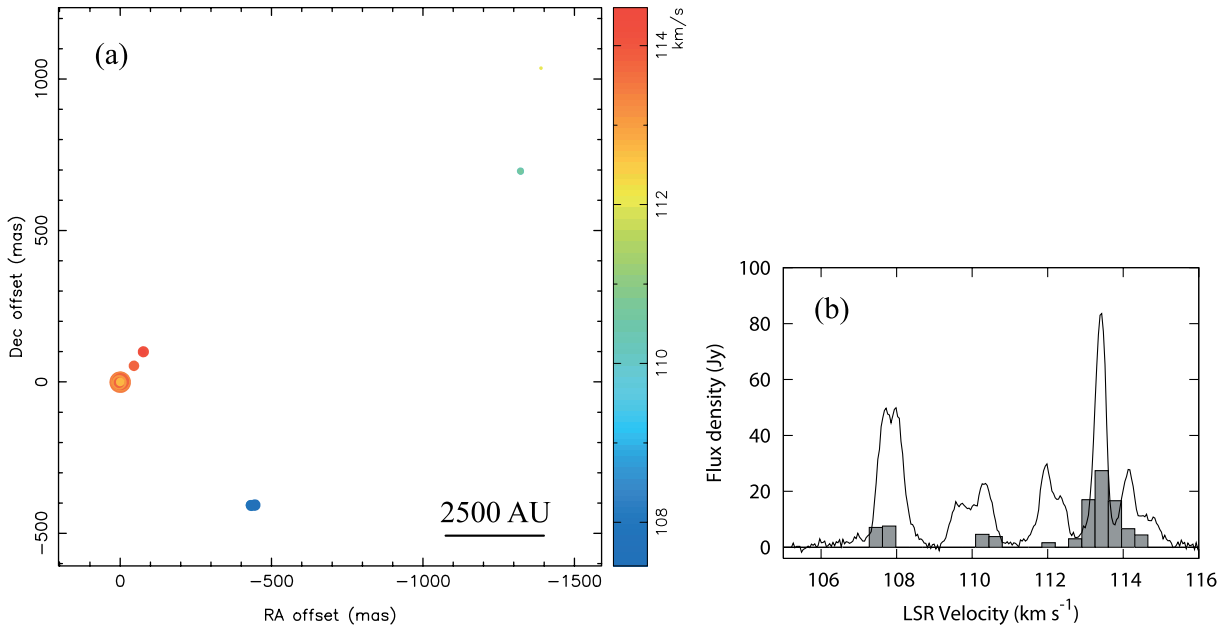

Fig. 6. G 24.78+0.08: (a) Wide field view of a 1.″4 × 1.″4 map. (b) CLEANed component spectrum (filled block) and total spectrum (solid curve).

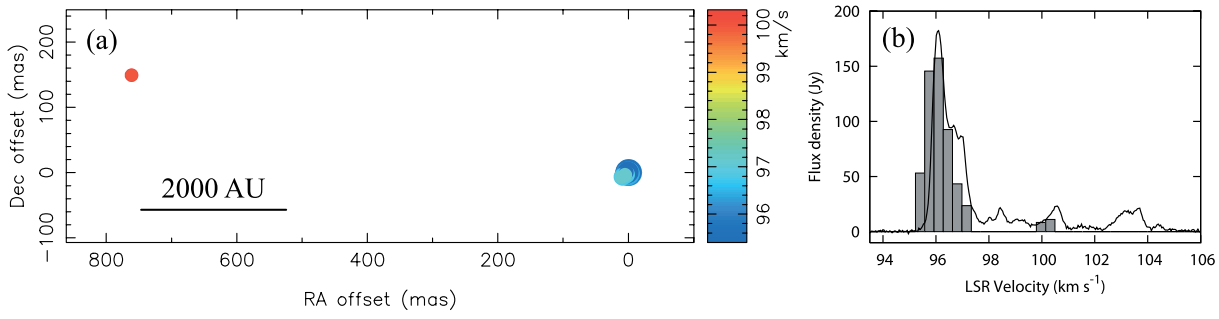

Fig. 7. G 29.95−0.02: (a) Wide field view of a 0.″76 × 0.″15 map. (b) CLEANed component spectrum (filled block) and total spectrum (solid curve).

source was observed with the ATCA (Beuther et al. 2002) and with the EVN (Voronkov et al. 2002). A spot of 27.83 km s^{-1}, 137 mas south of the main cluster, was newly detected.

3.6. G 24.78+0.08

G 24.78+0.08 (figure 6) is a cluster of massive protostars at a distance of 7.7 kpc (Forster & Caswell 1989). A pair of cores associated with a compact bipolar outflow have been detected (Furuya et al. 2002). Beltrán et al. (2004) have detected rotating disks associated with high-mass YSOs by observing the 1.4 mm continuum and CH_3CN (J = 12–11) line emission. The first VLBI image of methanol masers at 6.7 GHz of this source is obtained by our observation. This source consists of three clusters separated by more than 3000 AU.

3.7. G 29.95−0.02

G 29.95−0.02 (figure 7) is at a distance of 9 kpc (Wood & Churchwell 1989), and coincides with an NH_3 hot core, but is a few arcsec away from the continuum peak of a UC H II region (Cesaroni et al. 1998). The methanol masers of G 29.95−0.02 have been observed with the ATCA at 6.7 GHz (Walsh et al. 1998) and with the VLBA at 12.2 GHz (Minier et al. 2000, 2001). Our observation at 6.7 GHz shows the first VLBI image of this source, in which fourteen spots were detected. Twelve of them were clustered within 10 mas, and the other two spots were isolated 0.″76 east of the main cluster. These two clusters detected in our map correspond to M and G defined by Walsh et al. (1998). There are several spectral features between 95 and 105 km s^{-1}; in contrast to the 12.2 GHz spectrum, most of the weak features could not be detected by our VLBI observation.

3.8. IRAS 18556+0136

IRAS 18556+0136 (figure 8) is at a distance of 2 kpc (Brown et al. 1982), and is associated with CO outflows (Dent et al. 1985). Our VLBI observation is the first one of this source, and six maser spots were detected. This source consists of two clusters that are separated by more than 5000 AU. Although there are several spectral peaks, most of the weak features could not be detected.

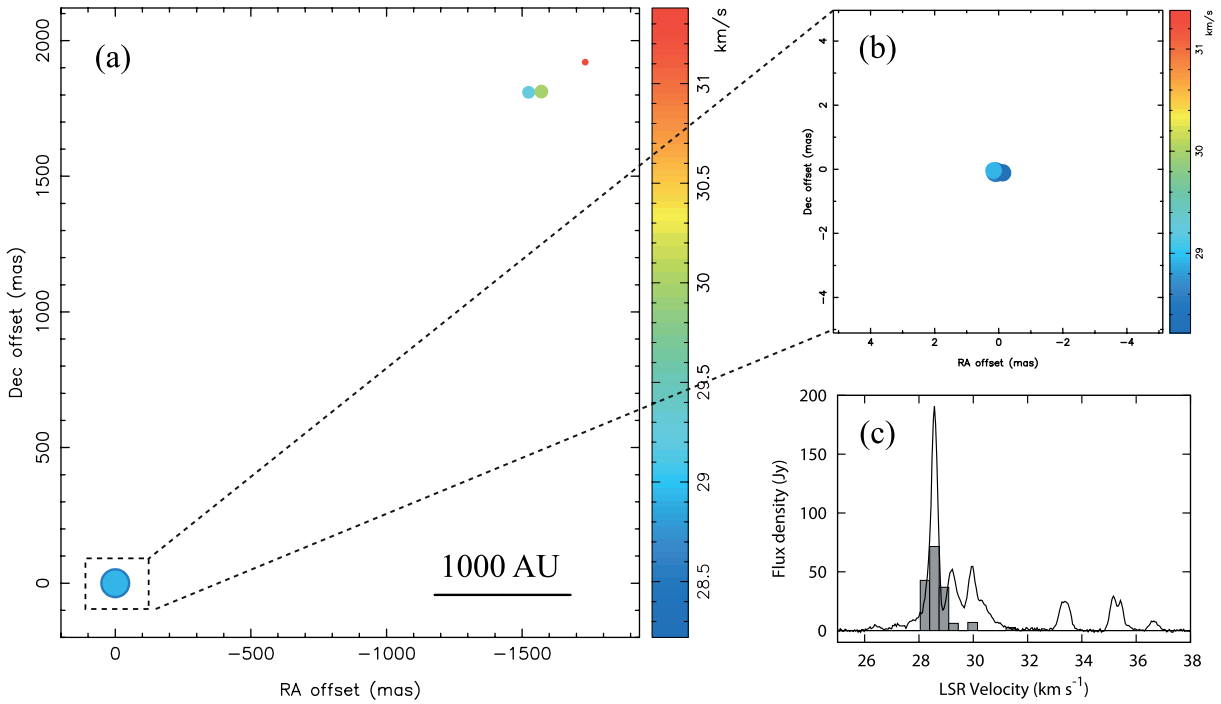

Fig. 8. IRAS 18556+0136: (a) Wide field view of a 1.″7 × 1.″9 map. (b) CLEANed component spectrum (filled block) and total spectrum (solid curve).

3.9. W 48

W 48 (figure 9) is a well-known H II region at a distance of 3.4 kpc (Vallee & Avery 1990). This source has a bright UC H II region that could be ongoing massive star formation (Wood & Churchwell 1989). W 48 have been observed with the EVN at 6.7 GHz (Minier et al. 2000) and with the VLBA at 12.2 GHz (Minier et al. 2000). The maser of this source is strong, and the spectrum is widespread; 24 spots forming a ringlike structure were detected, as observed by Minier et al. (2000). A spot of 43.86 km s^{-1}, 34 mas north and 55 mas west from the reference spot, was newly detected by this observation.

3.10. OH 43.8−0.1

OH 43.8−0.1 (figure 10) is a star-forming region at a distance of 2.8 ± 0.5 kpc (Honma et al. 2005). This star-forming region coincides with IRAS 19095+0930, which is a UC H II region (Kurtz et al. 1994). This is the first VLBI observation at 6.7 GHz for this source, and we detected nine maser spots. A spot of 43.00 km s^{-1} was located 0.″4 east and 0.″3 south from the reference spot.

3.11. ON 1

Onsala 1 (ON 1, figure 11) is a UC H II region located in the densest part of the Onsala molecular cloud (Israel & Wootten 1983). This source is known to be associated with a massive star-forming region and IRAS 20081+3122. A kinematic distance of 1.8 kpc is used by MacLeod et al. (1998) and Kumar, Tafalla, and Bachiller (2004). Our observation is the first VLBI at 6.7 GHz, and seven maser spots were detected. The redshifted and blueshifted clusters are separated about 1700 AU from each other. It is surprising that the redshifted cluster corresponds to the narrow (∼ 0.5 km s^{-1}) spectral maximum with a flux density of 107 Jy; the correlated flux density is only 4.6 Jy. The flux ratio of the correlated to the total spectra is 4.3%. On the other hand, the blueshifted cluster corresponds to a relatively weak (∼ 20 Jy) and wide spectral peak, while the flux ratio is about 50%.

3.12. Cep A

Cepheus A (Cep A, figure 12) is a CO condensation at a distance of 730 pc (Johnson 1957). One of the massive star-forming regions in Cep A is a UC H II region, CepA-HW 2 (Hughes & Wouterloot 1984). Cep A has been observed at 12.2 GHz with the VLBA (Minier et al. 2000, 2001), while our observation is the first VLBI at 6.7 GHz. We found 30 maser spots, 20 of which had $V_{\rm lsr}$ ranging from −1.15 to −3.26 km s^{-1}, and the other 10 spots had $V_{\rm lsr}$ ranging from −3.61 to −4.67 km s^{-1}. It is notable that spots in the redshifted cluster are aligned linearly. The blueshifted cluster is located 1.″34 east of the redshifted cluster.

3.13. NGC 7538

The NGC 7538 (figure 13) is a star-forming region at a distance of 2.8 kpc (Blitz et al. 1982; Campbell & Thompson 1984) including at least 11 high-luminosity infrared sources (NGC 7538 IRS 1−11), which are probably young massive stars (Kameya et al. 1990). Since the central star has been thought to be O6 (Willner 1976; Campbell & Thompson 1984), the luminosity of the central source is 8.3×10^4 $L_\odot$ and the mass is $\simeq$ 30 $M_\odot$. It is known that this object is associated with a UC H II region that is observed with the Very Large Array (VLA: Campbell 1984; Gaume et al. 1995). The

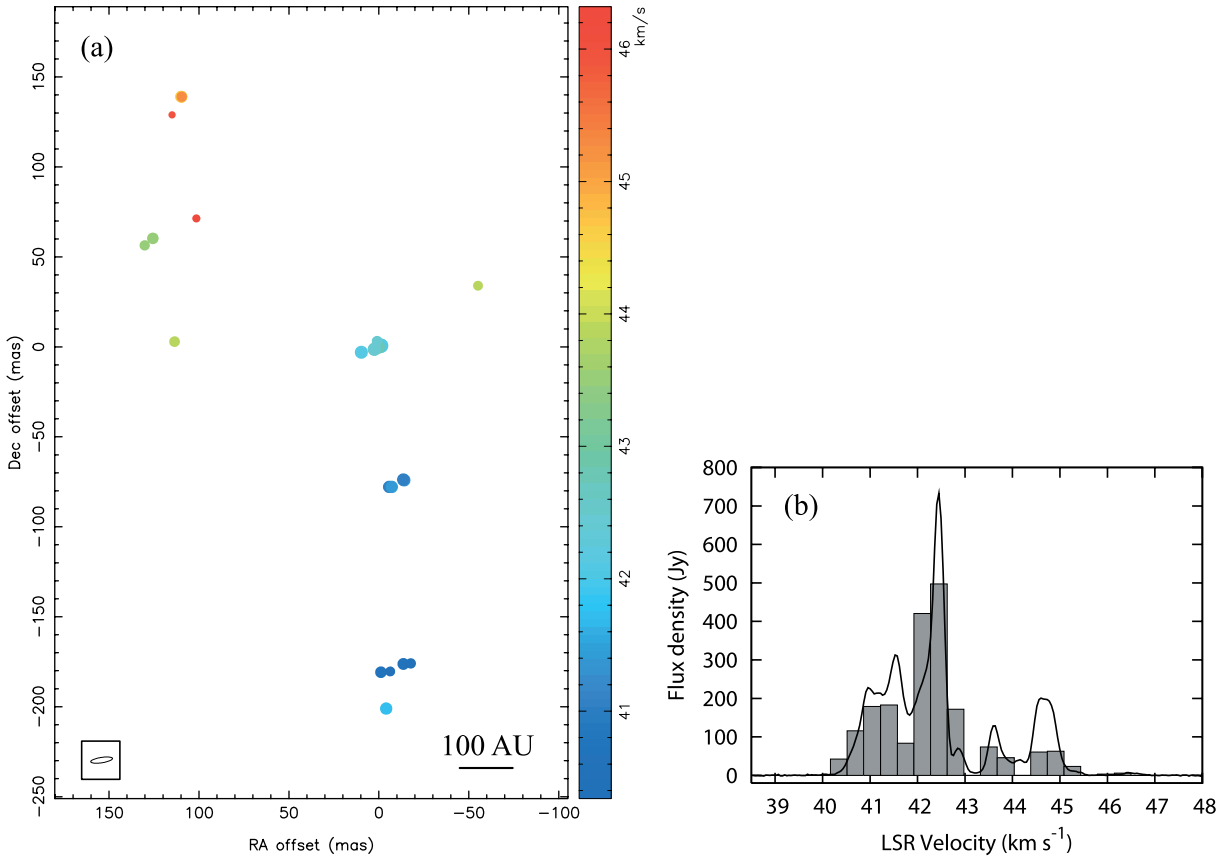

Fig. 9. W 48: (a) Map. (b) CLEANed component spectrum (filled block) and total spectrum (solid curve).

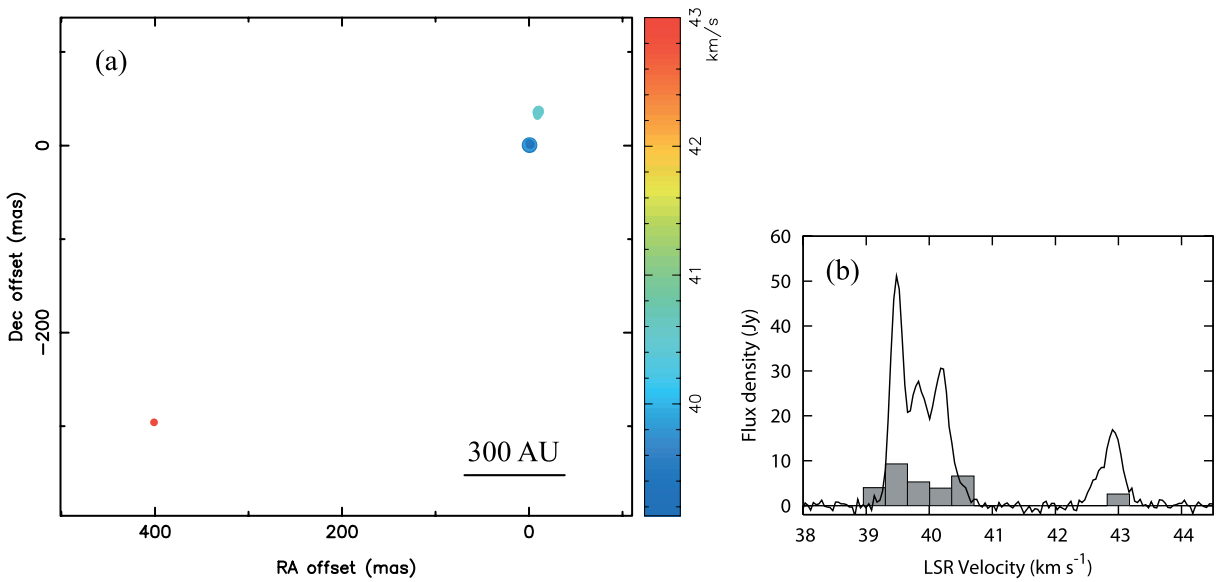

Fig. 10. OH 43.8−0.1: (a) Wide field view of a 0.″4 × 0.″3 map. (b) CLEANed component spectrum (filled block) and total spectrum (solid curve).

methanol maser of NGC 7538 has been observed with the MERLIN (Pestalozzi et al. 2006) and the EVN at 6.7 GHz (Minier et al. 1998, 2000, 2001; Pestalozzi et al. 2004, 2006), and with the VLBA at 12.2 GHz (Minier et al. 1998, 2000, 2001). The distribution of maser spots in our map corresponds to the IRS 1 region (Minier et al. 1998). The map is in agreement with that of Minier, Booth, and Conway (2000). The redshifted spots with $V_{\rm lsr}$ ranging from −56.45

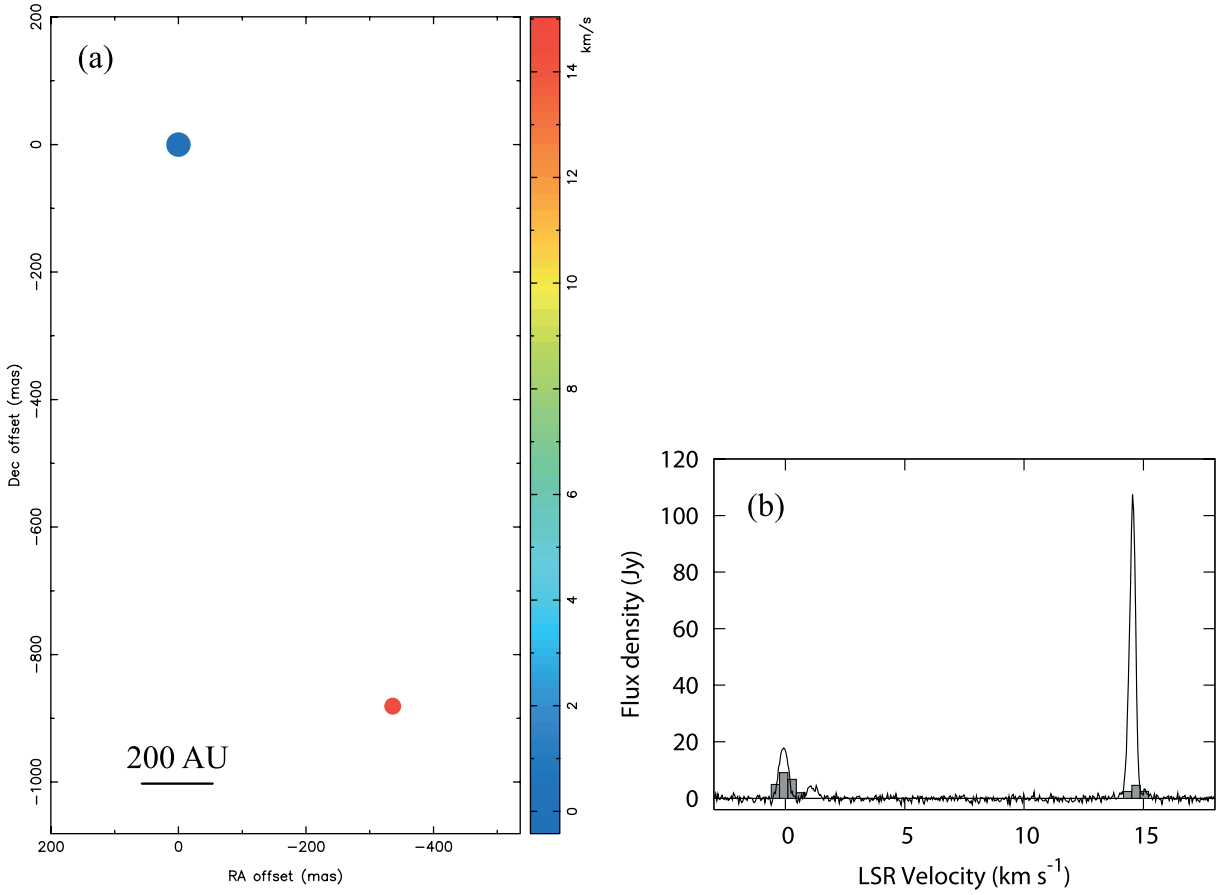

Fig. 11. ON 1: (a) Wide field view of a $0.''34 \times 0.''88$ map. (b) CLEANed component spectrum (filled block) and total spectrum (solid curve).

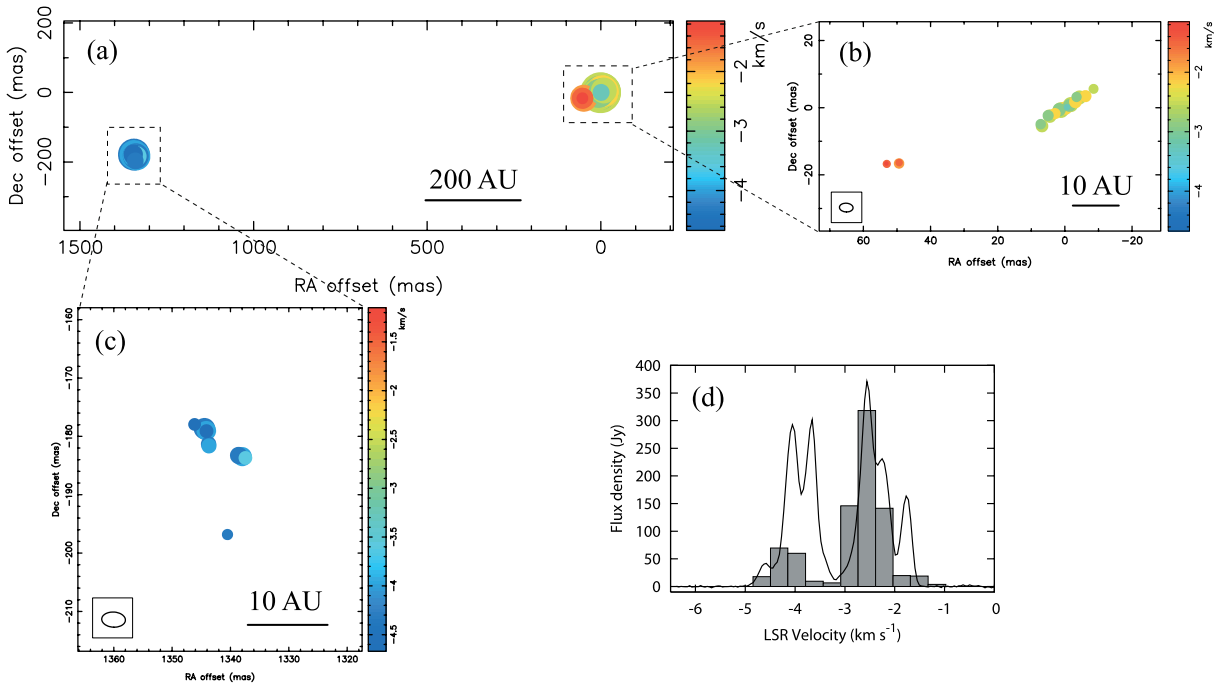

Fig. 12. Cep A: (a) Wide field view of a $1.''3 \times 0.''18$ map. (b) Close-up of the redshifted cluster. (c) Close-up of the blueshifted cluster. (d) CLEANed component spectrum (filled block) and total spectrum (solid curve).

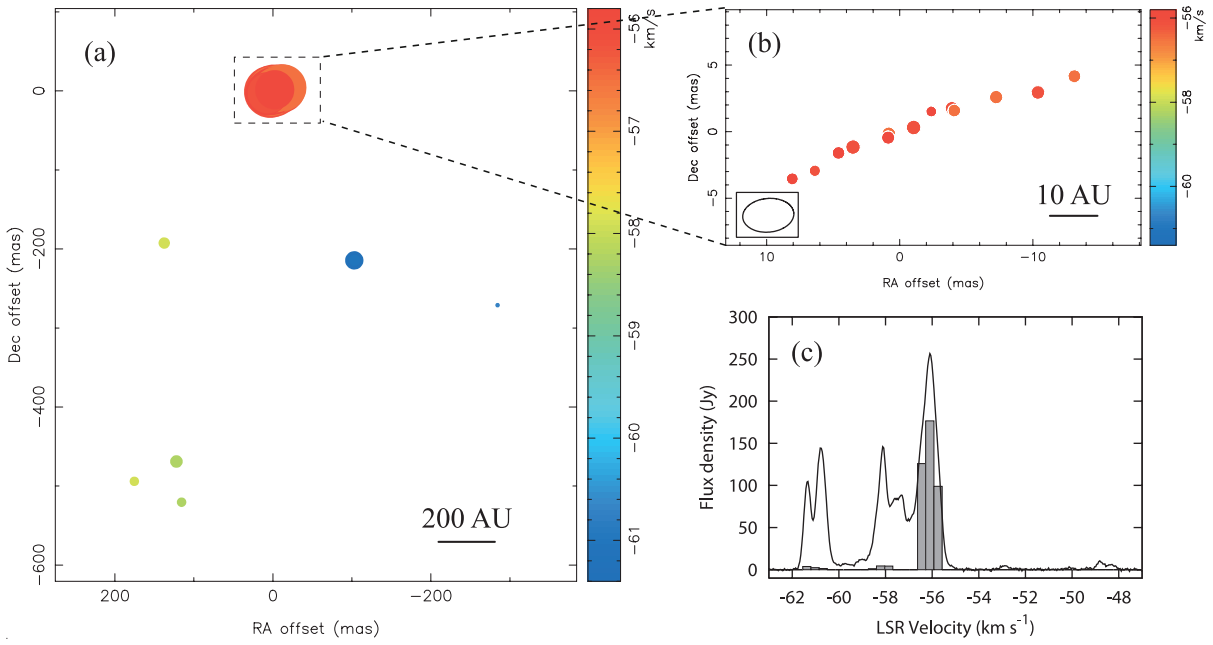

Fig. 13. NGC 7538: (a) Wide field view of a $0\farcs5 \times 0\farcs5$ map. (b) Close-up of the redshifted cluster. (c) CLEANed component spectrum (filled block) and total spectrum (solid curve).

to $-55.75\,\mathrm{km\,s^{-1}}$ are aligned linearly, as shown in previous studies (Minier et al. 1998; Pestalozzi et al. 2004). The spectral features of $-53.07\,\mathrm{km\,s^{-1}}$ and $-48.99\,\mathrm{km\,s^{-1}}$ corresponding to the infrared sources IRS 11 and IRS 9 (Pestalozzi et al. 2006), respectively, were not detected.

4. Discussions

We have presented maps of twelve sources of methanol maser emission; seven of them are the first VLBI results at 6.7 GHz. The spatial distributions of maser spots show various morphology, such as linear structures (Cep A NGC 7538), a ringlike structure (W 48), and very separated clusters [W 3(OH), W 33A, G 24.78+0.08, G 29.95−0.02, IRAS 18556+0136, OH 43.8−0.1, ON 1, and Cep A].

We discuss the properties of a methanol maser at 6.7 GHz as a possible probe for astrometry compared with the methanol maser at 12.2 GHz and the water maser at 22 GHz. We detected twelve out of thirteen methanol masers at 6.7 GHz, with the longest baseline being 50 Mλ of our array. The integrated flux densities of the correlated spectra account for $\sim$50% of the total flux, and some of them account for more than 90%. This high detection rate, flux recovery, and small fringe spacing of 4 mas suggest that most of the methanol maser emission has compact structures. This result is consistent with a previous study of W 3(OH) by Menten et al. (1992). We also showed that the correlated flux density at 50 Mλ is typically 20% of the total flux density. The size of the maser spot inferred from the flux ratio varies from 2 to 30 AU (at a distance from 0.73 to 9 kpc of the sources). This is consistent with the core size of 2 to 20 AU obtained by Minier, Booth, and Conway (2002). The velocity range of typically $10\,\mathrm{km\,s^{-1}}$ (Caswell et al. 1995a) is narrow as compared with that of water masers. Given this compactness and the narrow velocity range, as well as the known properties of long life and small internal motion, this methanol maser line is suitable for astrometry with VLBI.

From the viewpoint of the observation, the atmospheric fluctuation is a significant problem for observations at higher frequency. Strong absorption by water vapor in the atmosphere makes observations relatively difficult at 22 GHz in the summer. This would be a potential problem in measuring the annual parallax. This is not the case with the 6.7 GHz observation.

The astrometric VLBI observation uses continuum reference sources, which are usually distant quasars. Such continuum sources show power-law, decreasing spectra and the flux density is larger at 6.7 GHz than that of 12.2 GHz or 22 GHz. These properties make the astrometric observation easier in terms of the detectability of reference sources.

The 6.7 GHz line might have some disadvantages due to its lower frequency in compared with the 12.2 GHz line. The interstellar scintillation broadens the sizes of the maser and the reference source. The interstellar broadening is stronger at lower frequency, and might affect the precise positions of the sources. Also, the ionospheric density fluctuation changes the path length, and consequently affects a phase measurement at lower frequency. These effects depend on the frequency as ν^{-2}, i.e., the effect on the 6.7 GHz line is 3.3 times larger than on the 12.2 GHz. Although Minier, Booth, and Conway (2002) discussed that the interstellar broadening is not significant in the case of a scale larger that 1 mas, we should take account of these effects on astrometry.

We made a phase-referencing VLBI observation with the JVN, and achieved a positional accuracy of $\sim 50\,\mu$as at 8.4 GHz, and a image dynamic range of $\sim$50 on a target (Doi et al. 2006b). The bigradient phase referencing (BPR) was used for this observation, and a reference calibrator was separated by $2\fdg1$ from the target source. The following equation (1) can be

used to derive an accuracy $\Delta\pi$ of the annual parallax:

$$\Delta\pi = \frac{\theta_{\rm beam}}{D \cdot \sqrt{N_{\rm spot} \cdot N_{\rm obs}}}, \quad (1)$$

where $\theta_{\rm beam}$ is the minimum fringe spacing, D the dynamic range of the image, $N_{\rm spot}$ the number of spots used in measuring the annual parallax, and $N_{\rm obs}$ the number of observations. If we make a series of observations of nine methanol maser spots for five epochs, as in the cases of the observations by Xu et al. (2006), it is expected that an accuracy of $\sim 12\,\mu$as in the annual parallax could be achieved.

The flux density at 6.7 GHz is typically ~ 10 times larger than that at 12.2 GHz (Caswell et al. 1995b), and the number of observable sources of 6.7 GHz is much larger than that of 12.2 GHz. For this practical reason we choose the 6.7 GHz line rather than the 12.2 GHz one.

We have started to improve the JVN at 6.7 GHz in terms of the sensitivity and the number of stations to detect weak masers and reference sources. Usuda 64 m telescope is one of the newly participating ones. Assuming an aperture efficiency of 50% and a system noise temperature of 50 K for all of the telescopes, it is expected that the sensitivity to fringe detection (7σ) would be less than 5 Jy. We showed that the correlated flux density at 50 Mλ is typically 20% of the total flux density. Hence, sources with a total flux density of larger than 25 Jy would be potential targets for astrometric observation. The number of such sources found in the catalog by Pestalozzi, Minier, and Booth (2005) is greater than 150.

Note added in proof (2008 January 28): A VLBI image of G 24.78+0.08 is recently reported by Moscadelli et al. (2007, A&A, 472, 867).

The authors wish to thank the JVN team for observing assistance and support. The JVN project is led by the National Astronomical Observatory of Japan (NAOJ), which is a branch of the National Institutes of Natural Sciences (NINS), Hokkaido University, Gifu University, Yamaguchi University, and Kagoshima University, in cooperation with Geographical Survey Institute (GSI), the Japan Aerospace Exploration Agency (JAXA), and the National Institute of Information and Communications Technology (NICT).

References

Bartkiewicz, A., Szymczak, M., & van Langevelde, H. J. 2005, A&A, 442, L61
Batrla, W., Matthews, H. E., Menten, K. M., & Walmsley, C. M. 1987, Nature, 326, 49
Beckwith, S., Evans, N. J., II, Becklin, E. E., & Neugebauer, G. 1976, ApJ, 208, 390
Beltrán, M. T., Cesaroni, R., Neri, R., Codella, C., Furuya, R. S., Testi, L., & Olmi, L. 2004, ApJ, 601, L187
Beuther, H., Walsh, A., Schilke, P., Sridharan, T. K., Menten, K. M., & Wyrowski, F. 2002, A&A, 390, 289
Blitz, L., Fich, M., & Stark, A. A. 1982, ApJS, 49, 183
Brand, J., & Blitz, L. 1993, A&A, 275, 67
Bronfman, L., Nyman, L.-Å., & May, J. 1996, A&AS, 115, 81
Brown, A. T., Little, L. T., Macdonald, G. H., & Matheson, D. N. 1982, MNRAS, 201, 121
Campbell, B. 1984, ApJ, 282, L27
Campbell, B., & Thompson, R. I. 1984, ApJ, 279, 650
Caswell, J. L., Vaile, R. A., Ellingsen, S. P., & Norris, R. P. 1995b, MNRAS, 274, 1126
Caswell, J. L., Vaile, R. A., Ellingsen, S. P., Whiteoak, J. B., & Norris, R. P. 1995a, MNRAS, 272, 96
Cesaroni, R., Hofner, P., Walmsley, C. M., & Churchwell, E. 1998, A&A, 331, 709
Cragg, D. M., Johns, K. P., Godfrey, P. D., & Brown, R. D. 1992, MNRAS, 259, 203
Davis, C. J., Varricatt, W. P., Todd, S. P., & Ramsay Howat, S. K. 2004, A&A, 425, 981
Dent, W. R. F., Little, L. T., Kaifu, N., Ohishi, M., & Suzuki, S. 1985, A&A, 146, 375
Doi, A., et al. 2006a, in Proc. 8th European VLBI Network Symp. (Torun), p.71
Doi, A., et al. 2006b, PASJ, 58, 777
Dreher, J. W., & Welch, W. J. 1981, ApJ, 245, 857
Ellingsen, S. P. 2006, ApJ, 638, 241
Etoka, S., Cohen, R. J., & Gray, M. D. 2005, MNRAS, 360, 1162
Forster, J. R., & Caswell, J. L. 1989, A&A, 213, 339
Furuya, R. S., Cesaroni, R., Codella, C., Testi, L., Bachiller, R., & Tafalla, M. 2002, A&A, 390, L1
Gaume, R. A., Goss, W. M., Dickel, H. R., Wilson, T. L., & Johnston, K. J. 1995, ApJ, 438, 776
Genzel, R., et al. 1981b, ApJ, 247, 1039
Genzel, R., Reid, M. J., Moran, J. M., & Downes, D. 1981a, ApJ, 244, 884
Goddi, C., Moscadelli, L., Sanna, A., Cesaroni, R., & Minier, V. 2007, A&A, 461, 1027
Goedhart, S., Gaylard, M. J., & van der Walt, D. J. 2004, MNRAS, 355, 553
Greisen, E. W. 2003, in Information Handling in Astronomy – Historical Vistas, ed. A. Heck (Dordrecht: Kluwer Academic Publishers), 109
Hachisuka, K., et al. 2006, ApJ, 645, 337
Harvey-Smith, L., & Cohen, R. J. 2006, MNRAS, 371, 1550
Herbst, W., & Racine, R. 1976, AJ, 81, 840
Honma, M., et al. 2005, PASJ, 57, 595
Hughes, V. A., & Wouterloot, J. G. A. 1984, ApJ, 276, 204
Israel, F. P., & Wootten, H. A. 1983, ApJ, 266, 580
Johnson, H. L. 1957, ApJ, 126, 121
Joint IRAS Science W. G. 1988, Infrared Astronomical Satellite (IRAS) Catalog and Atlas (Washington, D.C.: NASA)[1]
Kameya, O., Morita, K.-I., Kawabe, R., & Ishiguro, M. 1990, ApJ, 355, 562
Kobayashi, H., et al. 2003, ASP Conf. Ser., 306, 367
Kumar, M. S. N., Tafalla, M., & Bachiller, R. 2004, A&A, 426, 195
Kurtz, S., Churchwell, E., & Wood, D. O. S. 1994, ApJS, 91, 659
Lonsdale, C. J., et al. 1998, BAAS, 30, 1355
MacLeod, G. C., Scalise, E. Jr., Saedt, S., Galt, J. A., & Gaylard, M. J. 1998, AJ, 116, 1897
Menten, K. M. 1991a, ASP Conf. Ser., 16, 119
Menten, K. M. 1991b, ApJ, 380, L75

[1] Joint IRAS Science W.G. 1994, VizieR Online Data Catalog, 2125, 0

Menten, K. M., Reid, M. J., Moran, J. M., Wilson, T. L., Johnston, K. J., & Batrla, W. 1988, ApJ, 333, L83
Menten, K. M., Reid, M. J., Pratap, P., Moran, J. M., & Wilson, T. L. 1992, ApJ, 401, L39
Mezger, P. G., Chini, R., Kreysa, E., Wink, J. E., & Salter, C. J. 1988, A&A, 191, 44
Minier, V., Booth, R. S., & Conway, J. E. 1998, A&A, 336, L5
Minier, V., Booth, R. S., & Conway, J. E. 2000, A&A, 362, 1093
Minier, V., Booth, R. S., & Conway, J. E. 2002, A&A, 383, 614
Minier, V., Conway, J. E., & Booth, R. S. 2001, A&A, 369, 278
Moscadelli, L., Menten, K. M., Walmsley, C. M., & Reid, M. J. 1999, ApJ, 519, 244
Moscadelli, L., Menten, K. M., Walmsley, C. M., & Reid, M. J. 2002, ApJ, 564, 813
Moscadelli, L., Menten, K. M., Walmsley, C. M., & Reid, M. J. 2003, ApJ, 583, 776
Pandian, J. D., Goldsmith, P. F., & Deshpande, A. A. 2007, ApJ, 656, 255
Patel, N. A., Greenhill, L. J., Herrnstein, J., Zhang, Q., Moran, J. M., Ho, P. T. P., & Goldsmith, P. F. 2000, ApJ, 538, 268
Pestalozzi, M. R., Elitzur, M., Conway, J. E., & Booth, R. S. 2004, ApJ, 603, L113
Pestalozzi, M. R., Minier, V., & Booth, R. S. 2005, A&A, 432, 737
Pestalozzi, M. R., Minier, V., Motte, F., & Conway, J. E. 2006, A&A, 448, L57
Racine, R. 1968, AJ, 73, 233
Shepherd, M. C. 1997, ASP Conf. Ser., 125, 77
Shibata, K. M., Kameno, S., Inoue, M., & Kobayashi, H. 1998, ASP Conf. Ser., 144, 413
Sobolev, A. M., Cragg, D. M., & Godfrey, P. D. 1997, MNRAS, 288, L39
Stier, M. T., et al. 1984, ApJ, 283, 573
Szymczak, M., Hrynek, G., & Kus, A. J. 2000, A&AS, 143, 269
Torrelles, J. M., et al. 2001a, ApJ, 560, 853
Torrelles, J. M., et al. 2001b, Nature, 411, 277
Turner, J. L., & Welch, W. J. 1984, ApJ, 287, L81
Vallee, J. P., & Avery, L. W. 1990, A&A, 233, 553
van der Tak, F. F. S., van Dishoeck, E. F., Evans, N. J., II, & Blake, G. A. 2000, ApJ, 537, 283
Vlemmings, W. H. T., Harvey-Smith, L., & Cohen, R. J. 2006, MNRAS, 371, L26
Vlemmings, W. H. T., van Langevelde, H. J., Diamond, P. J., Habing, H. J., & Schilizzi, R. T. 2003, A&A, 407, 213
Voronkov, M. A., Slysh, V. I., Palagi, F., & Tofani, G. 2002, Proceedings of the 6th EVN Symposium, 213
Walsh, A. J., Burton, M. G., Hyland, A. R., & Robinson, G. 1998, MNRAS, 301, 640
Willner, S. P. 1976, ApJ, 206, 728
Wood, D. O. S., & Churchwell, E. 1989, ApJ, 340, 265
Xu, Y., Reid, M. J., Zheng, X. W., & Menten, K. M. 2006, Science, 311, 54